Check for updates

IMMUNOLOGY

The lactate dehydrogenase (LDH) isoenzyme spectrum enables optimally controlling T cell glycolysis and differentiation

Xuyong Chen, Lingling Liu†, Siwen Kang†, JN Rashida Gnanaprakasam, Ruoning Wang*

Copyright © 2023 The Authors, some rights reserved; exclusive licensee American Association for the Advancement of Science. No claim to original U.S. Government Works. Distributed under a Creative Commons Attribution NonCommercial License 4.0 (CC BY-NC).

Isoenzyme divergence is a prevalent mechanism governing tissue-specific and developmental stage-specific metabolism in mammals. The lactate dehydrogenase (LDH) isoenzyme spectrum reflects the tissue-specific metabolic status. We found that three tetrameric isoenzymes composed of LDHA and LDHB (LDH-3/4/5) comprise the LDH spectrum in T cells. Genetically deleting *LDHA* or *LDHB* altered the isoenzyme spectrum by removing all heterotetramers and leaving T cells with LDH-1 (the homotetramer of LDHB) or LDH-5 (the homotetramer of LDHA), respectively. Accordingly, deleting *LDHA* suppressed glycolysis, cell proliferation, and differentiation. Unexpectedly, deleting *LDHB* enhanced glycolysis but suppressed T cell differentiation, indicating that an optimal zone of glycolytic activity is required to maintain cell fitness. Mechanistically, the LDH isoenzyme spectrum imposed by LDHA and LDHB is necessary to optimize glycolysis to maintain a balanced nicotinamide adenine dinucleotide/nicotinamide adenine dinucleotide hydrogen pool. Our results suggest that the LDH isoenzyme spectrum enables "Goldilocks levels" of glycolytic and redox activity to control T cell differentiation.

INTRODUCTION

Gene duplication drives the evolution of isoenzymes that differ in polypeptide sequences, quaternary structures, and catalytic efficiencies but catalyze the same biochemical reactions (*1*). The species-specific features of isoenzymes may reflect how the species biochemically adapts to environmental conditions (*2*). Within a single organism, the isoenzyme's pattern (spectrum) divergence fine-tunes metabolic activities to meet the need of a specific tissue or developmental stage. T cell–dependent immune response is energetically costly and requires an optimal glucose-derived carbon allocation to support rapid expansion and differentiation. The isoenzyme spectrum may play a critical role in shaping the T cell metabolic profile, characterized by high aerobic glycolysis and increased glutaminolysis but decreased fatty acid β-oxidation (FAO) after activation (*3*–*5*). Lactate dehydrogenase (LDH) controls the last step of glycolysis by catalyzing the coupled interconversion of pyruvate to lactate and nicotinamide adenine dinucleotide hydrogen (NADH) to nicotinamide adenine dinucleotide (NAD^+). Besides allosteric regulation, substrate-level regulation, and gene expression regulation, LDH has five predominant isoenzymes (LDH-1 to LDH-5), each with distinct catalytic properties (*6*). The LDH isoenzyme spectrum reflects glucose metabolism status in different organs such as the muscle, liver, and heart. However, the LDH isoenzyme spectrum in T cells and its potential impact on T cell–mediated immune response remain unclear. Therefore, we sought to examine the T cell–specific LDH isoenzyme spectrum in mice.

Center for Childhood Cancer and Blood Diseases, Hematology/Oncology and BMT, Abigail Wexner Research Institute at Nationwide Children's Hospital, The Ohio State University, Columbus, OH, USA.
*Corresponding author. Email: ruoning.wang@nationwidechildrens.org
†These authors contributed equally to this work.

RESULTS

The LDH isoenzyme spectrum in T cells is characterized by distinct homotetramer and heterotetramers comprising LDHA and LDHB

While the LDH zymography assay could not quantitatively evaluate the enzymatic activities because isoenzymes have different substrate affinity and catalytic coefficient, it reliably and qualitatively assessed the isoenzyme composition (spectra). The zymography of LDH revealed that the thymus exhibits a similar LDH isoenzyme spectrum as the heart, with nearly all five isoenzymes present; however, the spleen and the lymph node have one dominant isoenzyme (LDH-5) and two minor isoenzymes (LDH-4 and LDH-3) (Fig. 1A). To assess the isoenzyme spectrum in T cells, we isolated T cells from various lymphoid organs and examined their zymography pattern. Similar to the pattern revealed in tissue, T cells in the thymus exhibit five isoenzymes, whereas T cells in the spleen and the lymph node only have LDH-3, LDH-4, and LDH-5 (Fig. 1B). LDH isoenzymes are homotetramers or heterotetramers of the translational products of the *LDHA* gene and the *LDHB* gene (*6*). T cell receptor (TCR) activation increased LDHA but reduced LDHB expression, rendering the LDH-1 the dominant isoenzyme (Fig. 1C and fig. S1, A and B). Similarly, various CD4 T cell subsets all have LDH-5 as the dominant isoenzyme (fig. S1C). We have previously shown that transcriptional factors Myc and hypoxia-inducible factor 1α (HIF-1α) control glycolysis during T cell activation and differentiation by regulating metabolic gene expression (*7*, *8*). However, neither *Myc* deletion nor *HIF-1α* deletion changes the LDH isoenzyme spectrum in T cells (fig. S1, D and E), indicating that the intrinsic properties of LDHA and LDHB proteins determine the isoenzyme spectrum. Next, we assessed each gene product's role in regulating the LDH isoenzyme spectrum and enzymatic activities. Specifically, we generated T cell–specific *LDHA*, *LDHB*, and *LDHA/B* double knockout (DKO) strains [*LDHA* conditional knockout (cKO), *LDHB* cKO, and *LDHA/B* DKO] by crossing the CD4-Cre strain with the $LDHA^{fl}$ strain and $LDHB^{fl}$ strain separately or consecutively. LDH gene deletion did not result in defects in T cell development in the

Downloaded from https://www.science.org on April 09, 2025

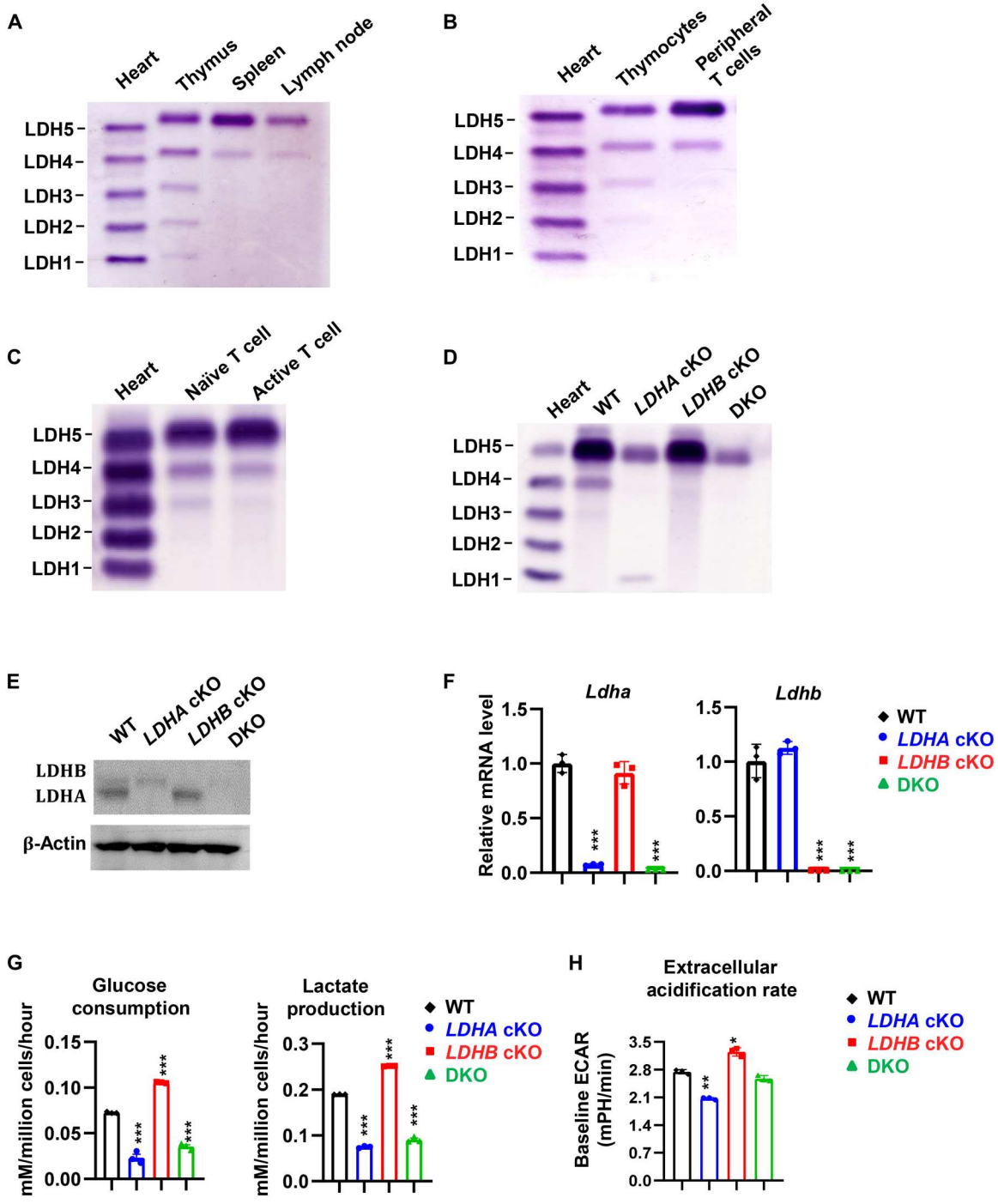

Fig. 1. The LDH isoenzyme spectrum in T cells is characterized by distinct homotetramer and heterotetramers comprising LDHA and LDHB. (**A** to **D**) LDH isoenzyme spectrum of the indicated tissues and cells was determined by zymography using the QuickGel system. (**E** and **F**) Protein or mRNA level of *LDHA* and *LDHB* of the indicated cells was determined by immunoblots or quantitative polymerase chain reaction. (**G**) After 3 days of activation, the blank and spent media were collected from T cells with indicated genotypes. The bioanalyzer (YSI 2900) quantified the indicated metabolites. The difference between blank and spent media determined the consumption and production of indicated metabolites. (**H**) T cells with indicated genotypes were activated for 24 hours, and the extracellular acidification rate (ECAR) was determined by Seahorse XF96 Analyzer. Data represent means ± SD ($n = 3$) for each group; experiments were repeated twice. *$P < 0.05$, **$P < 0.01$, and ***$P < 0.001$, one-way analysis of variance (ANOVA). cKO, conditional knockout; DKO, double knockout; WT, wild type.

Downloaded from https://www.science.org on April 09, 2025

thymus, spleen, and lymph nodes (fig. S2, A and B). Deleting *LDHA* leads to the loss of LDH-3 to LDH-5 but the formation of LDHB homotetramer isoenzyme LDH-1. Conversely, deleting *LDHB* leads to the loss of LDH-3 and LDH-4 without affecting LDH-5, the LDHA homotetramer isoenzyme. Deleting both genes abolishes all the isoenzymes (Fig. 1D). Notably, a weak LDH-5 signal remained in the *LDHA* cKO and *LDHA/B* DKO samples (Fig. 1D). To exclude the possibility that LDHA is incompletely deleted, we validated the deficiency of mRNA and protein by quantitative polymerase chain reaction (qPCR) and immunoblot analysis, respectively (Fig. 1, E and F). We reasoned that the weak staining signal overlapping with the LDH-5 position in the *LDHA* cKO and *LDHA/B* DKO samples is the sample loading background because LDH-5 has the slowest electrophoretic mobility and appears in the sample loading area. Because deleting either *LDHA* or *LDHB* changed the LDH spectra in T cells, we reasoned that their deletion would compromise glycolysis upon T cell activation under a proximately physiological relevant oxygen level (around 5% O_2) supplied in vitro (*9*). *LDHA* cKO or *LDHA/B* DKO T cells displayed a reduced glycolysis flux compared to wild-type (WT) T cells after activation, as indicated by decreased glucose consumption, lactate production, and extracellular acidification rates (ECARs) (Fig. 1, G and H). Unexpectedly, deleting *LDHB* enhanced glucose consumption, lactate production, and ECAR in T cells after activation (Fig. 1, G and H). Our results show that thymic and periphery T cells exhibit distinct isoenzyme spectra. Altering the LDH isoenzyme spectrum by *LDHA* or *LDHB* deletion resulted in opposite effects on changing glycolysis.

Altering the LDH isoenzyme spectrum affects T cell proliferation and differentiation in vivo

We hypothesized that deleting *LDHA* would suppress T cell proliferation, whereas deleting *LDHB* would enhance proliferation because heightened glycolysis is necessary for driving T cell proliferation after activation (*7*, *10*). We assessed the impact of altering the LDH isoenzyme spectrum on $CD4^+$ T cells in vivo. We first used a well-established competitive homeostatic proliferation assay to determine the ratio and carboxyfluorescein succinimidyl ester (CFSE) dilution pattern of purified WT(*Thy1.1*$^+$), *LDHA* cKO, *LDHB* cKO, or *LDHA/B* DKO(*Thy1.2*$^+$) $CD4^+$ T cells in a lymphopenic host ($Rag^{-/-}$). Unexpectedly, altering the isoenzyme spectrum by deleting either *LDHA* alone or *LDHB* alone is sufficient to dampen cell proliferation and viability. However, *LDHA* cKO cells exhibit more profound defects than *LDHB* cKO cells (Fig. 2, A to C). As expected, deleting both *LDHA* and *LDHB* genes loses all five isoenzymes, almost abolishing cell proliferation and viability, as evidenced by the cell ratio between DKO and WT and the CFSE dilution pattern (Fig. 2, A to C).

Next, we measured antigen-specific, TCR-dependent proliferation and differentiation of T cells by modulating the LDH isoenzyme spectrum. Because DKO completely abolishes the LDH isoenzyme spectrum, we focused on *LDHA* or *LDHB* cKO in the experiment. We crossed *Thy1.1* and CD4-Cre, *LDHA*^{fl} or *LDHB*^{fl} mice with OVA-specific T-cell receptor (OT-II) transgenic mice to generate OT-II, WT(*Thy1.1*$^+$), OT-II, LDHA cKO(*Thy1.2*$^+$), and OT-II, *LDHB* cKO(*Thy1.2*$^+$) donor strains in $CD45.2^+$ background. We then adoptively transferred mixed and CFSE-labeled WT and cKO $CD4^+$ T cells into $CD45.1^+$ mice immunized with chicken ovalbumin ($OVA_{323–339}$). Consistent with the homeostatic proliferation results, altering the isoenzyme spectrum by deleting either *LDHA* or *LDHB* led to proliferation defects in an antigen-specific manner after immunization. In addition, *LDHA* cKO cells have more severe proliferation defects than *LDHB* cKO cells (Fig. 2, D to F). *LDHA* or *LDHB* deletion resulted in fewer IFN-γ^+CD4^+ T cells and IL-17^+CD4^+ T cells than the WT group, indicating that altering the isoenzyme spectrum influences T cell differentiation (Fig. 2G and fig. S3, A and B).

Experimental autoimmune encephalomyelitis (EAE) is an inflammatory demyelinating disease mouse model and is primarily driven by the proinflammatory T cells [T helper 1 (T_H1) and T_H17] in the central nervous system (CNS). Genetically deleting *LDHA* in T cells confers protection against EAE's pathogenic progression (*11*). We used this well-characterized system to investigate the in vivo $CD4^+$ T cell response by altering the LDH isoenzyme spectrum by deleting the *LDHA* or *LDHB* gene. In line with our homeostatic and antigen-specific proliferation results, deleting *LDHA* or *LDHB* in T cells conferred protection against the pathogenic progression of EAE mice, accompanied by decreased CD4+IFN-γ+ and CD4+IL-17+did not change the percentage of $CD4^+FoxP3^+$ cells in the CNS, while deleting *LDHA* increased its percentage (fig. S3, C and D). These findings suggest that the optimal LDH isoenzyme spectrum conferred by LDHA and LDHB is required to sustain T cell expansion and differentiation in vivo. Thus, altering the isoenzyme spectrum by deleting either *LDHA* or *LDHB* dampens the metabolic fitness of T cells and hence causes proliferation and differentiation defects in vivo.

Altering the LDH isoenzyme spectrum affects T cell proliferation and differentiation in vitro

After examining the role of LDH in regulating T cells in vivo, we used a range of in vitro functional assays to investigate how altering the LDH isoenzyme spectrum affects T cell phenotypes. In vitro cell culture studies were conducted under 5% O_2 at approximately physiologically relevant oxygen levels to resemble the effects of modulating LDH and glycolysis on T cell functions in vivo (*9*). Compared with WT $CD4^+$ T cell, *LDHA* and *LDHA/B* deletion caused more cell death (fig. S4, A and B) and delayed cell cycle progression from G_0/G_1 to S phase (fig. S4C) upon activation in vitro, which were associated with reduced cell surface activation markers (fig. S4D), moderately reduced cell size (fig. S4E), and RNA/DNA/protein contents (fig. S4, F to G). By contrast, deleting *LDHB* did not cause any of these effects, indicating that LDHB is dispensable in controlling T cell activation in vitro (fig. S4, A to G).

Next, we mixed CFSE-labeled WT(*Thy1.1*$^+$) $CD4^+$ T cells with *LDHA* cKO, *LDHB* cKO, or *LDHA/B* DKO(*Thy1.2*$^+$) $CD4^+$ T cells at a 1:1 ratio and followed cell ratio and proliferation in the competitive setting after activation. In line with the in vivo results, altering the LDH isoenzyme spectrum by deleting *LDHA*, *LDHB*, or both genes reduced the cell number and the ratio of KO to WT in a time-dependent manner (Fig. 3, A to C). While deleting *LDHA* or *LDHB* only marginally reduced CFSE dilution in $CD4^+$ T cells, deleting both genes substantially reduced CFSE dilution (Fig. 3D).

Next, we examined the effects of altering the LDH isoenzyme spectrum on T_H1 and T_H17 and induced regulatory T cell (iT_{reg}) differentiation. Consistent with the recent studies (*11*, *12*), *LDHA* deletion substantially suppressed T_H1 and T_H17 differentiation (Fig. 3E). In line with the results from the OT-II experiment (Fig. 2G), deleting *LDHB* reduced the percentage of IFN-γ^+CD4^+

Downloaded from https://www.science.org on April 09, 2025

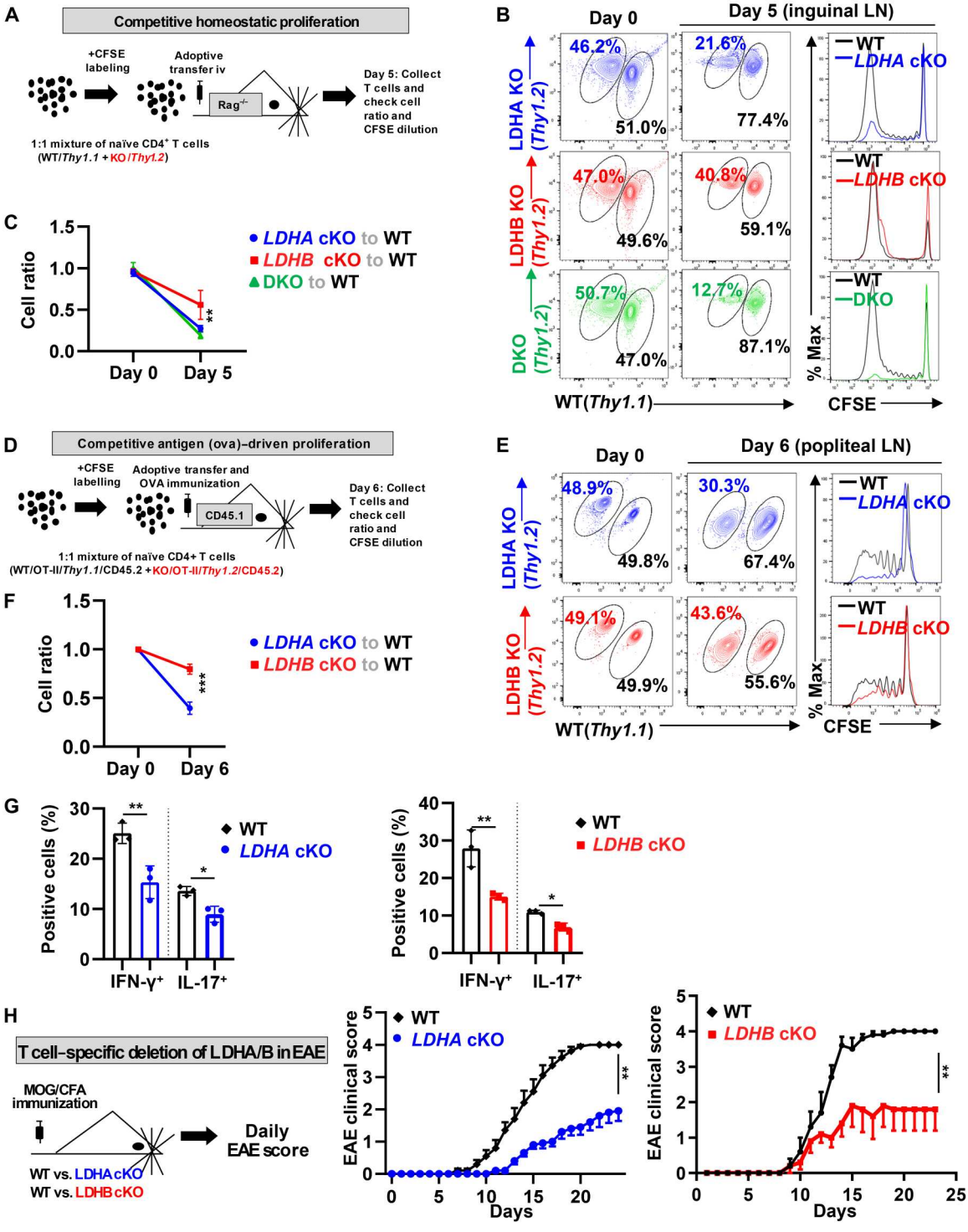

Fig. 2. The optimized isoenzyme spectrum requires LDHA and LDHB to sustain T cell expansion and inflammation in vivo. (**A** and **D**) Diagrams of the indicated experimental procedures. (**B** to **G**) Donor $CD4^+$ T cell ratios before and after adoptive transfer were determined by surface staining of isogenic markers. Cell proliferation was determined by CFSE dilution, and the indicated cytokines were determined by intracellular staining. (**H**) Diagram of experimental autoimmune encephalomyelitis (EAE) procedure (left); clinical scores were evaluated daily (middle and right). Data represent means ± SD ($n = 3$ to 5) for each group, and experiments were repeated twice. *$P < 0.05$, **$P < 0.01$, and ***$P < 0.001$, one-way ANOVA and two-way ANOVA. CFA, complete Freund adjuvant; IFN-γ, interferon-γ; IL-17, interleukin-17; LN, lymph node; MOG, myelin oligodendrocyte glycoprotein.

Downloaded from https://www.science.org on April 09, 2025

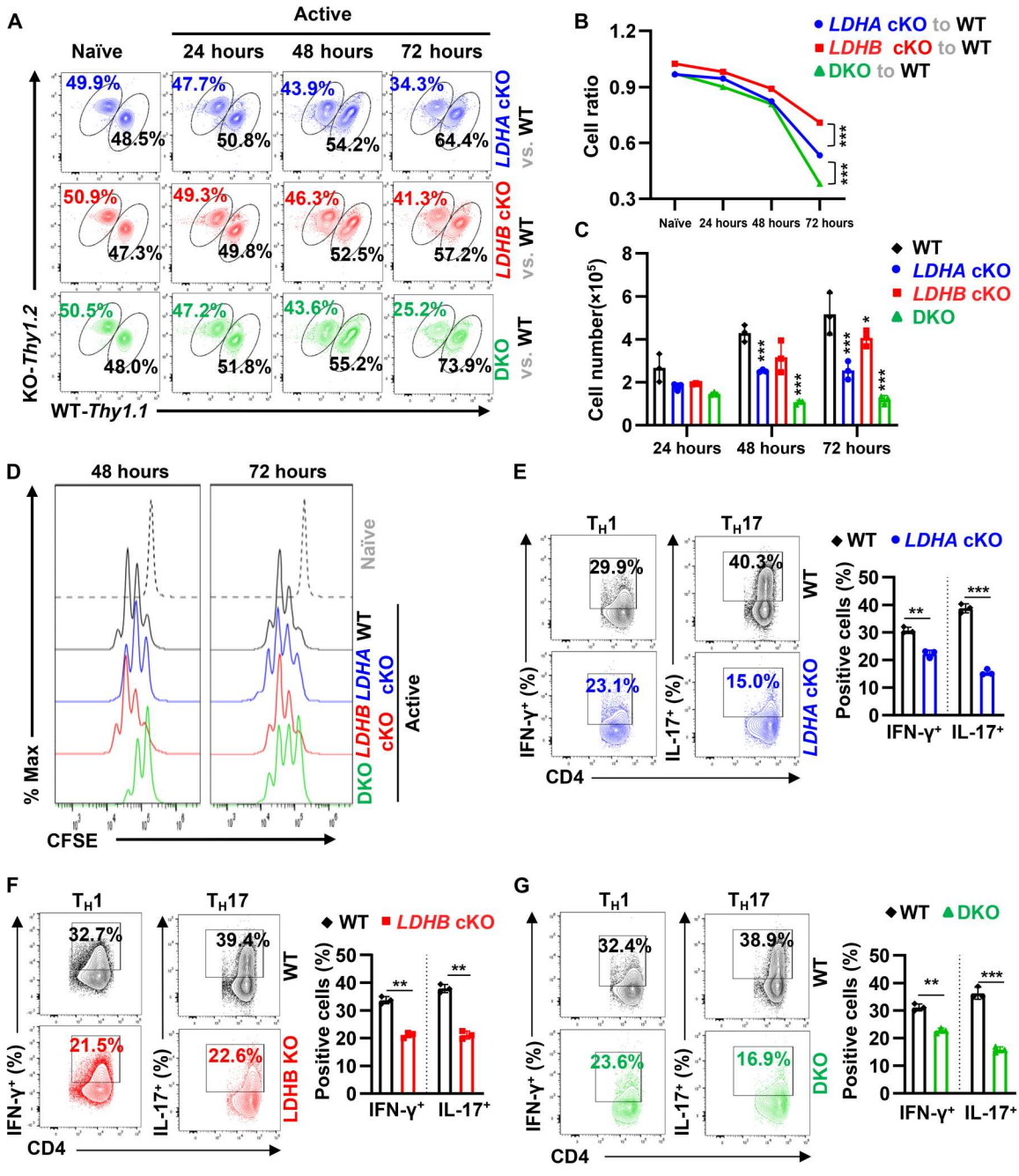

Fig. 3. Altering the LDH isoenzyme spectrum affects T cell proliferation and differentiation in vitro. (**A** to **D**) CD4$^+$ T cells with indicated genotypes were mixed with a 1:1 ratio and activated in vitro. At the indicated time points, the cell ratio was determined by surface staining of isogenic markers (A and B), cell number was determined by the cell counter (C), and cell proliferation was determined by CFSE dilution (D). Data represent three independent experiments. *P < 0.05 and ***P < 0.001, one-way ANOVA. (**E** to **G**) CD4$^+$ T cells with indicated genotypes were polarized toward T_H1 and T_H17 lineages for 72 hours. The indicated proteins were quantified by intracellular staining. Data represent three independent experiments. **P < 0.01, and ***P < 0.001, one-way ANOVA, Student's t test. Data represent means ± SD (n = 3).

T cells and IL-17$^+$CD4$^+$ T cells under T_H1 and T_H17 polarization conditions, respectively (Fig. 3F). Similarly, deleting both *LDHA* and *LDHB* inhibited T_H1 and T_H17 differentiation (Fig. 3G). Deleting *LDHA* enhanced iT$_{reg}$ differentiation, but deleting *LDHB* cKO or DKO suppressed its differentiation (fig. S5A). Because the culture media formulation could shape T cell metabolism and functions (*13*, *14*), we sought to examine the impact of deleting *LDHB* on T cell differentiation using human plasma–like media (HPLM), which more closely resembles metabolite formulation in plasma (*15*). Similar to our findings based on RPMI 1640 media (Fig. 3F and fig. S5A), deleting *LDHB* reduced the differentiation of all CD4$^+$ T cell subsets when cells were cultured with HPLM media (fig. S5B). Our in vitro findings corroborate in vivo results, suggesting

Downloaded from https://www.science.org on April 09, 2025

that the optimal LDH isoenzyme spectrum is required to sustain T cell expansion and differentiation.

The Goldilocks principle conferred by the LDH isoenzyme spectrum enables a fine-tuned redox control of T cell differentiation

We and others have previously shown that T_H17 cells sustain high glycolysis, and inhibiting glycolysis suppresses T_H17 cell differentiation (*8*, *16*, *17*). We then determined how altering the LDH isoenzyme spectrum affects glycolysis and differentiation. As expected, deleting *LDHA* during T_H17 differentiation suppresses glucose consumption, lactate production, ECAR, and glycolysis (^3H_2O production from [5-^{3}H]-glucose at the triose phosphate isomerase reaction) (Fig. 4, A to D). By contrast, deleting *LDHB* during T_H17 differentiation resulted in an opposite pattern of changes in the above metabolic assays (Fig. 4, A to D). Specifically, altering the LDH isoenzyme spectrum by deleting *LDHB* enhances the overall glycolysis flux compared to WT control as indicated by an increased glucose consumption and lactate production (Fig. 4, A and B), a higher ECAR (Fig. 4C), and a heightened ^3H_2O production from [5-^{3}H]-glucose (Fig. 4D) (*18*). However, *LDHB* deletion did not change the overall glutamine consumption, glutamate production, glutaminolysis, and FAO (fig. S6, A to D). In addition, *LDHB* deletion did not alter these pathways′ metabolic gene expression profile (fig. S6, E to G).

The free cytosolic [NAD^+]/[NADH] ratio is crucial in ensuring cellular redox and energy homeostasis (*19*). Glycolysis determines the redox state of NAD^+/NADH in the cytoplasm through the action of glyceraldehyde-3-phosphate dehydrogenase and LDH (*20*). Next, we measured the cellular NAD^+/NADH ratio after altering the LDH isoenzyme spectrum. *LDHA* deletion or *LDHB* deletion in T cells decreased or increased the NAD^+/NADH ratio, respectively (Fig. 4E). To test whether the imbalance of NAD^+/NADH causes differentiation defects in *LDHA* and *LDHB* cKO cells, we added NADH to *LDHB* cKO cells and NAD^+ to *LDHA* cKO cells under T_H17 and T_H1 polarization conditions. The NADH supplement and NAD^+ supplement restored the balance of NAD^+/NADH and partially rescued differentiation defects in *LDHB* cKO and *LDHA* cKO, respectively (Fig. 4, F, G, I, and J, and fig. S7, A, B, D, and E). Altering the LDH isoenzyme spectrum also reduced cellular adenosine 5′-triphosphate (ATP) levels, which were restored after supplementing with NAD^+ or NADH in *LDHA* cKO and *LDHB* cKO cells (Fig. 4, H and K, and fig. S7, C and F). NAD^+ or NADH supplement did not affect T_H17 differentiation in *LDHB* cKO cells or *LDHA* cKO cells, respectively (fig. S7, G and H). Next, we examined the effect of NADH supplement on *LDHB* cKO T cell in the OT-II model as described early (Fig. 2D). The NADH supplement enhanced the percentage of the interferon-γ–positive (IFN-γ^+) and interleukin-17–positive (IL-17^+) *LDHB* cKO T cells without changing the cell ratio between WT and *LDHB* cKO T cells (fig. S8, A to C). These findings suggest that the LDH isoenzyme spectrum is required to maintain the redox state of NAD^+/NADH in T cells. Our results further indicate that the presence of the "Goldilocks zone" (not too high, not too low, but just right) may ensure the optimal glucose carbon input in determining the immunological outcomes quantitatively (Fig. 5).

DISCUSSION

T cell–mediated immune response in the vertebrate is energetically costly and often requires rapidly using and allocating available carbon resources. Hence, changing environments and rapidly evolving pathogens impose selective pressures on T cells, ensuring rapid metabolic changes upon activation. Accordingly, TCR stimulation immediately engages aerobic glycolysis, transforming carbon, and chemical energy to support T cell growth, proliferation, and differentiation (*18*, *21*–*25*). One of the largest constituents of the T cell proteome is the reservoir of highly abundant glycolytic enzymes, including LDHA and LDHB (*26*–*28*). Without changing transcriptional and translational states, a diverse and broad spectrum of LDH isoenzymes in T cells may permit a rapid glycolytic switch upon activation while maintaining some degrees of flexibility to optimize activities across a wide range of nutrient conditions and immunological contexts (*7*, *8*, *16*, *29*). The five LDH isoenzymes (LDH-1 to LDH-5) are tetrameric proteins arising from varying combinations of LDHA and LDHB. The LDH isoenzyme spectrum in central organs such as the muscle, liver, and heart reflects their metabolic profiles, particularly the glycolysis status. We have revealed that the LDH isoenzyme spectrum in periphery T cells consists of one homotetramer of LDHA (LDH-5) and two heterotetramers of LDHA and LDHB (LDH-3 and LDH-4). Despite their apparent redundancy, removing heterotetramers (LDH-3 and LDH-4) and leaving T cells with either LDH-1 (*LDHA* cKO) or LDH-5 (*LDHB* cKO) compromised T cell survival and differentiation substantially, suggesting that a diverse spectrum of the LDH isoenzyme confers the optimal metabolic fitness to T cell.

In the final step of glycolysis, LDH catalyzes the reversible conversion of pyruvate to lactate, coupled with the interconversion of NADH to NAD^+. Abrogating *LDHA* shifts the isoenzyme spectrum toward the LDH-1, reducing the overall glycolytic flux and decreasing effector T cell proliferation and differentiation. Shifting the LDH isoenzyme spectrum toward LDH-5 by *LDHB* deletion enhances glycolysis but still compromises T cell survival and differentiation. One biologically important principle is to avoid reaching the extreme but evolve toward optimization (*30*). Our findings suggest that glycolytic flux in T cells requires managing within certain margins, "not too high, not too low, but just right" (often called the Goldilocks principle), to ensure the optimal functional outcome in T cells.

Similarly, the optimal strength of TCR signaling governs how T cells transition between different states during development in the thymus, activation, and differentiation in the periphery (*31*, *32*). The Goldilocks zone of glycolysis reflects the T cell′s capacity to ensure proper functions with high metabolic efficiency. However, the boundaries of the Goldilocks zone may change as T cells transition between different states during activation and differentiation. Supporting this idea is the fact that different T cell subsets exhibit distinct glycolytic capacities (*8*, *16*, *33*).

Our studies revealed that altering one glycolytic enzyme′s isoenzyme spectrum is sufficient to tune up or down the overall glycolysis flux in T cells. The LDH activity not only is indispensable for sustaining glycolytic flux but also is critical for controlling the ratio of free cytosolic [NAD^+]/[NADH], which reflects the overall redox state in hyperproliferating cells such as active T cells and cancer cells (*19*, *20*, *34*–*37*). Because each isoenzyme exhibits a different

Downloaded from https://www.science.org on April 09, 2025

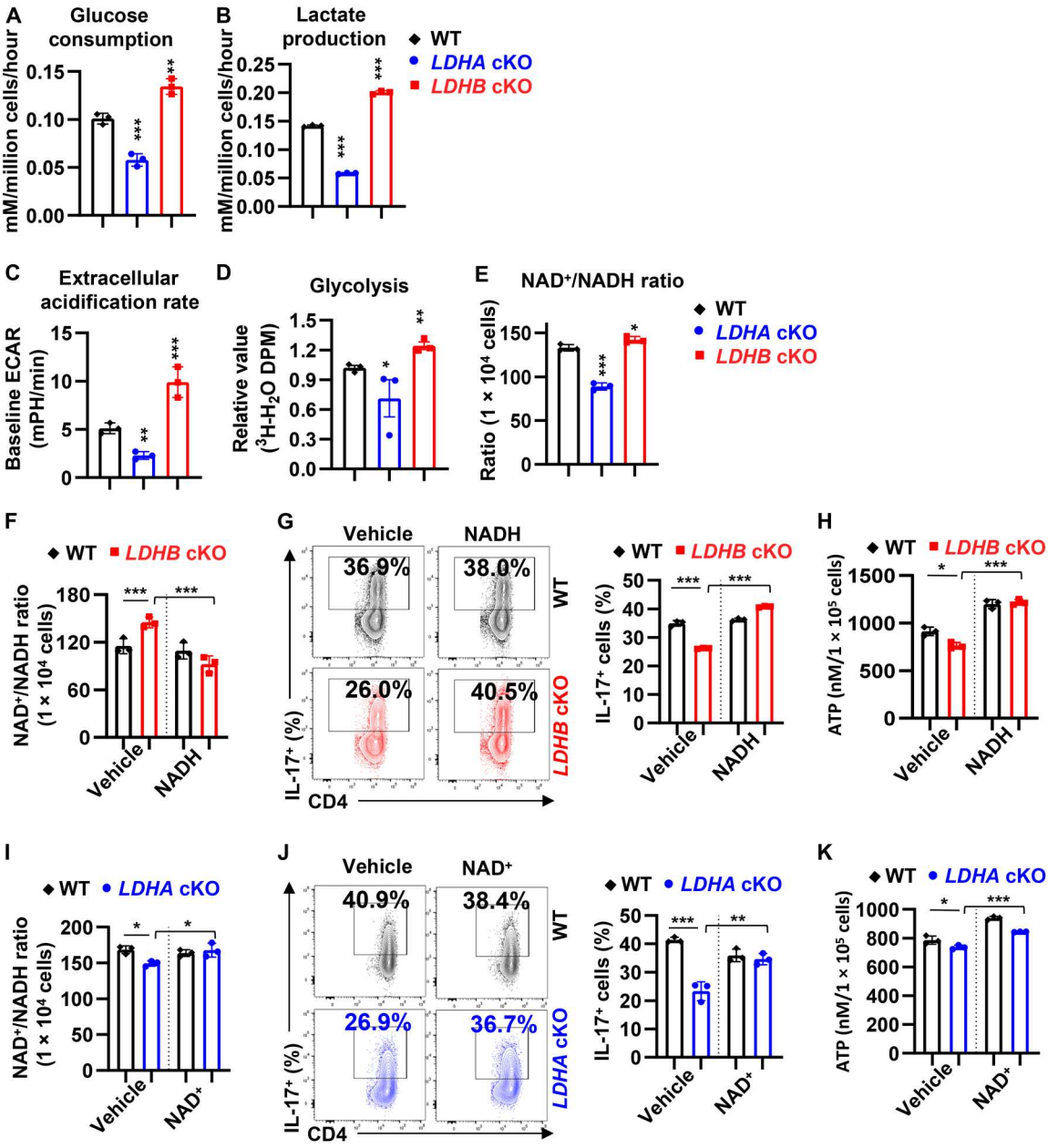

Fig. 4. LDH isoenzyme spectrum confers an optimal glycolytic flux to maintain the NAD$^+$/NADH ratio during T cell differentiation. (**A** and **B**) CD4$^+$ T cells with indicated genotypes were polarized toward T_H17 lineages for 2 days and then resuspended with fresh media. After 24 hours, blank media (without cells) and spent media (with cells) were collected. The bioanalyzer (YSI 2900) quantified the indicated metabolites. The difference between blank and spent media determined the metabolites' consumption and production. (**C** to **K**) CD4$^+$ T cells with indicated genotypes were polarized toward T_H17 lineages for 3 days, and the ECAR was measured by Seahorse XF96 Analyzer (C). The glycolysis rate was determined by generating ^3H_2O from [5-^{3}H]-glucose (D). The NAD/NADH-Glo Assay Kit (E, F, and I) measured the NAD$^+$/NADH ratio. Intracellular staining of IL-17 determined T_H17 differentiation (G and J), and the CellTiter-Glo 2.0 Assay Kit determined adenosine 5′-triphosphate levels (H and K). Data represent three independent experiments. *P < 0.05, **P < 0.01, and ***P < 0.001, one-way ANOVA. Data represent means ± SD (n = 3).

cofactor/substrate affinity, the composition of multiple LDH isoenzymes in T cells reflects an intrinsic constraint on maintaining the glycolytic rate within a given range and keeping the NAD$^+$/NADH ratio in check. Consequentially, the suboptimal glycolytic rate resulting from altering the isoenzyme spectrum leads to the imbalance of the NAD$^+$/NADH pool. The NAD$^+$/NADH redox state determines cellular redox balance and thus controls cellular homeostasis and fate (*38*, *39*).

Glycolysis also affects T cell redox homeostasis through other mechanisms. Glycolysis interconnects with the pentose phosphate pathway and, therefore, may influence the cytosolic ratio of NADP$^+$/NADPH, the other cellular redox couple. Through channeling its intermediate metabolite to glycine biosynthesis, glycolysis

Downloaded from https://www.science.org on April 09, 2025

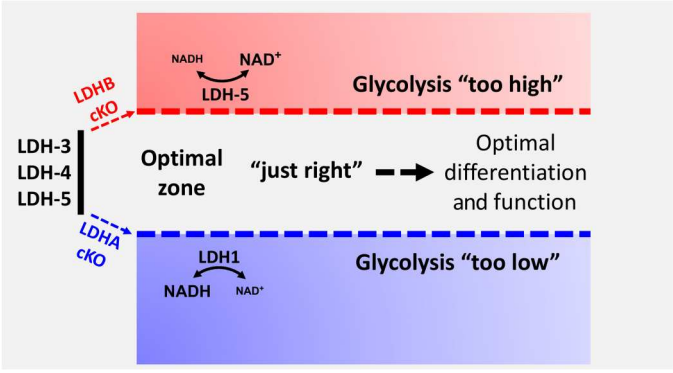

Fig. 5. The "Goldilocks principle" in regulating glycolysis and differentiation. Proposed conceptual model: The LDH isoenzyme spectrum enables "Goldilocks levels" of glycolytic and redox activity (i.e., not too high, not too low, but just right) to control the T cell differentiation function.

also contributes to producing glutathione, an essential antioxidant. The most critical role of LDH-dependent reaction is to preserve cytosolic NAD^+/NADH homeostasis under various cellular contexts (*40*, *41*). Supporting this idea, we have shown that restoring the ratio of NAD^+/NADH in LDH-1 dominant (*LDHA* cKO) T cells by NAD^+ supplement or in LDH-5 dominant (*LDHB* cKO) T cells by NADH supplement could partially rescue differentiation defects in these cells. Collectively, the LDH isoenzyme spectrum may evolve to ensure the optimal glycolytic rate range to maintain redox balance and support T cell function across a broad range of nutrient conditions and immunological contexts.

MATERIALS AND METHODS

Mice

C57BL/6NHsd (WT) mice, *Rag*$^{-/-}$ mice, OT-II mice, *Thy 1.1*$^+$ mice, *CD45.1*$^+$ and *Ldha*^{fl} mice, C57BL/6-*Il17a*^{tm1Bcgen}/J mice, and B6.129S4-*Ifng*$^{tm3.1Lky}$/J mice were obtained from the Jackson Laboratory (Bar Harbor, ME). The UC Davis Knockout Mouse Program (KOMP) repository generated the *Ldhb*$^{<tm1a(KOMP)Wtsi>}$ mice, which were further crossed with a transgenic Flippase strain [B6.129S4*Gt(ROSA)26Sor*$^{tm1(FLP1)Dym}$/RainJ] to remove the LacZ reporter allele to generate *LDHB*^{fl} mice. *LDHA*^{fl} mice and *LDHB*^{fl} mice were crossed with the CD4-Cre strain to generate T cell–specific *LDHB* knockout strain (*LDHB* cKO) or *LDHA* knockout strain (*LDHA* cKO). The *LDHA-LDHB* DKO mice were produced by crossing *LDHA* cKO mice with *LDHB* cKO mice. *HIF-1*α cKO and *c-MYC* KO mice were reported previously (*7*, *8*). OT-II mice [B6.Cg-Tg(TcraTcrb)425Cbn/J] were crossed with CD4-Cre *LDHA* cKO mice or CD4-Cre *LDHB* cKO mice to create the OT-II CD4-Cre *LDHA* cKO mice or OT-II CD4-Cre *LDHB* cKO mice. OT-II mice [B6.Cg-Tg(TcraTcrb)425Cbn/J] were crossed with *Thy1.1*$^+$ mice (B6.PL-*Thy1*a/CyJ) to generate OT-II *Thy1.1*(WT) mice. Mice with gender and age matched (7 to 12 weeks old) were used in the experiment. All mice were bred and kept in specific pathogen–free conditions at the Animal Center of Abigail Wexner Research Institute at Nationwide Children's Hospital. All animal protocols were approved by the Institutional Animal Care and Use Committee of the Abigail Wexner Research Institute at Nationwide Children's Hospital (protocol number AR13-00055).

Mouse T cell isolation and culture

All cells were cultured in RPMI 1640 media or HPLM supplemented with 10% (v/v) fetal bovine serum, 2 mM L-glutamine, 0.05 mM 2-mercaptoethanol, penicillin (100 U/ml), and streptomycin (100 μg/ml) at 37°C in 5% CO_2 and 5% O_2. Total $CD3^+$ T cells or naïve $CD4^+$ T cells were enriched from mouse spleen and lymph nodes by negative selection using the MojoSort Mouse CD3 T Cell Isolation Kit or the MojoSort Mouse CD4 Naïve T Cell Isolation Kit (MojoSort, BioLegend) following the manufacturer's instructions. For the activation assay, freshly isolated total murine T cells were either maintained in culture media with murine IL-7 (mIL-7) (5 ng/ml) for the resting state or were activated with mIL-2 (5 ng/ml). The culture plates were precoated with anti-mCD3 (2 μg/ml; clone 145-2C11, Bio X Cell) and anti-mCD28 (2 μg/ml; clone 37.51, Bio X Cell) antibodies overnight at 4°C. For $CD4^+$ T cell differentiation, 48-well culture plates were precoated with anti-mCD3 and anti-mCD28 antibodies (2 μg/ml for T_H1, T_H2, and iT_{reg} differentiation) or (4 μg/ml for T_H17 differentiation) overnight at 4°C. Freshly isolated naïve $CD4^+$ T cells (0.6×10^6/ml) were activated with plate-bound antibodies and mIL-2 (10 ng/ml) and mIL-12 (20 ng/ml) for T_H1 differentiation; with mIL-2 (2 ng/ml), mIL-4 (50 ng/ml), and anti–mouse IFN-γ (anti–mIFN-γ; 10 μg/ml) for T_H2 differentiation; with mIL-2 (3 ng/ml) and human transforming growth factor β1 (hTGF-β1; 10 ng/ml) for iT_{reg} differentiation; or with mIL-6 (50 ng/ml), hTGF-β1 (20 ng/ml), anti–mIL-2 (8 μg/ml), anti–mIL-4 (8 μg/ml), and anti–mIFN-γ (8 μg/ml) for T_H17 differentiation. In some experiments, 3 to 10 μM NADH or 0.1 μM NAD^+ added to cell culture media restored the intracellular NAD^+/NADH ratio. Additional information on cytokines, antibodies, and chemicals is listed in table S1.

Flow cytometry

For analyzing surface markers, cells were stained in phosphate-buffered saline (PBS) containing 2% (w/v) bovine serum albumin and the appropriate antibodies from BioLegend. For analyzing intracellular cytokine IFN-γ and IL-17A, T cells were stimulated for 4 hours with eBioscience Cell Stimulation Cocktail (eBioscience) before being stained with cell-surface antibodies. Cells were then fixed and permeabilized using FoxP3 Fixation/Permeabilization solution according to the manufacturer's instructions (eBioscience). CFSE staining assessed cell proliferation per the manufacturer's instructions (Invitrogen). 7-Aminoactinomycin D (7-AAD) staining assessed cell viability per the manufacturer's instructions (BioLegend). For analyzing DNA/RNA content, cells were collected and stained with surface markers before being fixed with 4% paraformaldehyde for 30 min at 4°C, followed by a permeabilization step with FoxP3 permeabilization solution (eBioscience). Cells were stained with 7-AAD for 5 min and then stained with pyronin Y (4 μg/ml) for 30 min before analysis by flow cytometer with peridinin-chlorophyll-protein (PerCP) detecting channel for 7-AAD (DNA) and phycoerythrin (PE) detecting channel for pyronin Y (RNA).

The protein synthesis assay kit (item no. 601100, Cayman) analyzed protein content. Briefly, cells were incubated with *O*-propargyl-puromycin for 1 hour, then were fixed, and stained with five carboxyfluorescein (FAM) azide staining solutions before analysis with a flow cytometer with the fluorescein isothiocyanate channel.

For analyzing the cell cycle profile, cells were incubated with 5-bromo-2′-deoxyuridine (BrdU) (10 μg/ml) for 1 hour, followed by

Downloaded from https://www.science.org on April 09, 2025

cell surface staining, fixation, and permeabilization according to the Phase-Flow Alexa Fluor 647 BrdU Kit (BioLegend). NovoCyte (ACEA Biosciences) acquired all flow cytometry data, which were analyzed with FlowJo software (TreeStar). Additional information on antibodies and dyes is listed in table S2.

LDH isoenzymes assay

The LDH isoenzymes assay was performed according to the manufacturer's instructions of the QuickGel LD Isoenzymes Kit (HELENA Laboratories, catalog no. 3338). Briefly, homogenized tissue or cell samples were diluted in the cold tris buffer (10 mM, pH 7.4) to quantify proteins. Samples (1 μg of protein each) were loaded on the agarose gel and electrophoresed for 5 min in the QuickGel chamber at 600 V. Then, the gel was removed from the chamber and stained with QuickGel LD isoenzyme reagent at 45°C for 20 min. The gel was washed with the destaining solution for 10 min and then with water for 5 min before being dried in the chamber and scanned for analysis.

NAD^+/NADH detection assay

The NAD^+/NADH ratios were analyzed according to the manufacturer's instructions for the NAD/NADH-Glo Assay Kit (Promega, catalog no. G9071). Briefly, 1×10^4 cells were suspended with 50 μl of PBS in 96-well white-walled tissue culture plates and an equal volume of NAD/NADH-Glo detection reagent. Samples were incubated at room temperature for 30 to 60 min. The Molecular Devices SpectraMax M2 Multilabel Microplate Reader (Marshall Scientific) measured the luminescence, and GraphPad Prism 9.0 analyzed the data.

ATP levels measurement

The ATP levels were measured according to the manufacturer's instructions of the CellTiter-Glo 2.0 Assay Kit (Promega, catalog no. G9241). Briefly, 1×10^5 cells were suspended with 50 μl of PBS in 96-well white-walled tissue culture plates and an equal volume of CellTiter-Glo 2.0 reagent. The plate was put on a shaker for gentle mixing and incubated at room temperature for 30 min. The Molecular Devices SpectraMax M2 Multilabel Microplate Reader (Marshall Scientific) measured luminescence, and GraphPad Prism 9.0 analyzed the data.

Glucose, lactate, glutamine, and glutamate quantification

The naïve $CD4^+$ T cells were polarized under T_H17 condition for 2 days before being collected and resuspended in fresh media at the density of 2×10^6/ml. Blank media (without cells) and spent media were collected after 24 hours. The bioanalyzer (YSI 2900) measured the metabolite levels. Calculating the difference between blank and spent media determined the metabolite consumption and production.

ECAR measurement

A Seahorse XFe96 Analyzer (Agilent Technologies) determined ECAR according to the manufacturer's manual. Briefly, 1.5×10^5 cells were suspended in Seahorse XF RPMI Assay media (with 2 mM glucose and 2 mM glutamine) and seeded in poly-D-lysine–precoated XF96 microplates. The plate was centrifuged to immobilize cells and kept in a non-CO_2 incubator for 30 min. A Seahorse XFe96 Analyzer (Agilent Technologies) measured the basal ECAR.

Western blot analysis

For protein extraction, cells were harvested, lysed, and sonicated at 4°C in a lysis buffer [50 mM tris-HCl (pH 7.4), 150 mM NaCl, 0.5% SDS, 5 mM sodium pyrophosphate, protease, and phosphatase inhibitor tablet]. Cell lysates were centrifuged at 13,000*g* for 15 min, and the supernatant was recovered. The Pierce BCA Protein Assay kit (Thermo Fisher Scientific) determined protein concentrations.

The samples were boiled in NuPAGE LDS Sample Buffer and reducing solution (Thermo Fisher Scientific) for 5 min. The proteins were separated by NuPAGE 4 to 12% Protein Gels (Thermo Fisher Scientific), transferred to polyvinylidene difluoride membranes by using the iBlot Gel Transfer Device (Thermo Fisher Scientific), and then incubated with primary antibodies (table S3), followed by incubating with the secondary antibodies conjugated with horseradish peroxidase. Immunoblots were developed on films using the enhanced chemiluminescence technique.

RNA extraction, reverse trascription qPCR, and RNA sequncing

The RNeasy Mini Kit (QIAGEN) was used for RNA isolation. Random hexamers and M-MLV Reverse Transcriptase (Invitrogen) were used for cDNA synthesis. The Bio-Rad CFX96 Real-Time PCR Detection System was used for SYBR Green–based qPCR. The relative gene expression was determined by the comparative cycle threshold (CT) method, also referred to as the $2^{-\Delta\Delta CT}$ method. The data were presented as the fold change in gene expression normalized to an internal reference gene (β2-microglobulin) and relative to the control (the first sample in the group). Fold change = $2^{-\Delta\Delta CT}$ = $[(CT_{\text{gene of interest}} - CT_{\text{internal reference}})]$ sample A − $[(CT_{\text{gene of interest}} - CT_{\text{internal reference}})]$ sample B. Samples for each experimental condition were run in triplicated PCR reactions. Primers detected target genes (table S4).

For RNA sequencing analysis, the total RNA was extracted using the RNeasy Mini Kit (QIAGEN) and treated with deoxyribonuclease I according to the manufacturer's instructions. After assessing the quality of total RNA using an Agilent 2100 Bioanalyzer and RNA Nanochip (Agilent Technologies), 150 ng of total RNA was treated to deplete the levels of ribosomal RNA (rRNA) using target-specific oligos combined with rRNA removal beads. Following rRNA removal, mRNA was fragmented and converted into double-stranded cDNA. Adaptor-ligated cDNA was amplified by limit cycle PCR. After library quality was determined via Agilent 4200 TapeStation and quantified by KAPA qPCR, approximately 60 million paired-end 150–base pair sequence reads were generated on the Illumina HiSeq 4000 platform. Quality control and adapter trimming were accomplished using the FastQC (version 0.11.3) and Trim Galore (version 0.4.0) software packages. Trimmed reads were mapped to the Genome Reference Consortium GRCm38 (mm10) murine genome assembly using TopHat2 (version 2.1.0), and feature counts were generated using HTSeq (version 0.6.1). Statistical analysis for differential expression was performed using the DESeq2 package (version 1.16.1) in R, with the default Benjamini-Hochberg *P* value adjustment method. The heatmap was generated using GraphPad Prism 9.0 software to show the differential expression of the selected genes.

Radioactive tracer–based metabolic assays

The metabolic assays were performed as described previously (*42*). Glycolysis was measured by the generation of ^3H_2O from [5-^{3}H(N)]

Downloaded from https://www.science.org on April 09, 2025

D-glucose, fatty acid oxidation was measured by the generation of ^3H_2O from [9,10-^{3}H] palmitic acid, and glutamine oxidation activity was measured by the generation of $^{14}CO_2$ from [U-^{14}C]-glutamine. For assays generating $^{14}CO_2$, 5 million T cells in 0.5 ml of fresh media were dispensed into 7-ml glass vials (TS-13028, Thermo Fisher Scientific) with a PCR tube containing 50 μl of 0.2 N NaOH glued on the sidewall. After adding 0.5-μCi radioactive tracer, a screw cap with a rubber septum (TS-12713, Thermo Fisher Scientific) sealed the vials, which were incubated at 37°C for 2 hours. Injecting 100 μl of 5 N HCl halted the assay, and vials were maintained at room temperate overnight to trap the $^{14}CO_2$. The NaOH in the PCR tube was then transferred to scintillation vials containing 10 ml of scintillation solution for counting. A cell-free sample containing 0.5-μCi [U-^{14}C]-glutamine served as a background control. For assays generating ^3H_2O, 1-μCi radioactive tracer was added to 1 million suspended cells in 0.5 ml of fresh media in 48 wells and then incubated at 37°C for 2 hours. The cells were transferred to a 1.5-ml microcentrifuge tube containing 50 μl of 5 N HCl and placed in 20-ml scintillation vials containing 0.5 ml of water with the vials capped and sealed. ^3H_2O was separated from other radio-labeled metabolites by evaporation diffusion overnight at room temperature. A cell-free sample containing 1-μCi radioactive tracer served as a background control.

Adoptive cell transfer assays

For homeostatic proliferation in lymphopenic *Rag*$^{-/-}$ mice, naïve CD4$^+$ T cells isolated from donor mice were mixed 1:1 with WT and KO cells and labeled with CFSE. Approximately, 1×10^7 cells in 150 μl of PBS were transferred via retro-orbital venous injection into 6- to 8-week-old gender-matched host mice. Mice were euthanized after 5 days, and lymph nodes were extracted from host mice and then processed for surface staining and flow analysis.

For antigen-driven proliferation using OT-II mice, naïve CD4$^+$ T cells isolated from OT-II/CD45.2 TCR transgenic donor mice were mixed with WT and KO cells at a 1:1 ratio and labeled with CFSE. Approximately, 1×10^7 cells in 150 μl of PBS were transferred via retro-orbital venous injection into 6- to 8-week-old gender-matched CD45.1 host mice. Host mice were immunized subcutaneously in the hock area (10 μl each site) in both legs with $OVA_{323–339}$ peptide (1 mg/ml; InvivoGen) emulsified with complete Freund adjuvant (CFA) (InvivoGen). CD45.1 host mice were intraperitoneally injected with NADH (400 mg/kg) (daily) in the indicated experiments. After 6 days of antigen-driven proliferation, lymph organs were extracted from host mice and processed for surface staining, intracellular staining, and flow analysis.

Experimental autoimmune encephalomyelitis

For induced EAE, mice were immunized subcutaneously with 100 μg of myelin oligodendrocyte glycoprotein ($MOG_{35–55}$) peptide emulsified in CFA, which was made from incomplete Freund adjuvant (Difco) plus *Mycobacterium tuberculosis* (Difco). Mice were intraperitoneally injected with 200 ng of pertussis toxin (List Biological Laboratories) on the day of immunization and 2 days later. The mice were observed daily for clinical signs and scored as described previously. (*8*)

In some experiments, mice were euthanized when control mice reached the onset of symptoms. The CNS (brain and spinal cord), spleen, and peripheral lymph nodes were collected and mashed to make a single-cell solution. The cell suspension was centrifuged on a 30%/70% Percoll gradient at 500*g* for 30 min to isolate mononuclear cells from the CNS, followed by cell surface staining and flow cytometric analysis.

Statistical analysis

Statistical analysis was conducted using the GraphPad Prism software version 9.0.0 (GraphPad Software Inc.). Unpaired two-tailed Student's *t* test and multiple one-/two-way analysis of variance (ANOVA) comparisons assessed the differences. $P < 0.05$ was considered significant, with $^*P < 0.05$, $^{**}P < 0.01$, and $^{***}P < 0.001$.

Supplementary Materials

This PDF file includes:

Figs. S1 to S8

Tables S1 to S4

View/request a protocol for this paper from *Bio-protocol*.

REFERENCES AND NOTES

1. H.-M. Eun, 1-Enzymes and nucleic acids general principles, in *Enzymology Primer for Recombinant DNA Technology* (Academic Press, 1996), pp. 1–108.
2. P. W. Hochachka, G. N. Somero, *Biochemical Adaptation: Mechanism And Process in Physiological Evolution* (Oxford Univ. Press, 2002).
3. R. Wang, D. R. Green, Metabolic checkpoints in activated T cells. *Nat. Immunol.* **13**, 907–915 (2012).
4. J. A. Shyer, R. A. Flavell, W. Bailis, Metabolic signaling in T cells. *Cell Res.* **30**, 649–659 (2020).
5. K. A. Frauwirth, J. L. Riley, M. H. Harris, R. V. Parry, J. C. Rathmell, D. R. Plas, R. L. Elstrom, C. H. June, C. B. Thompson, The CD28 signaling pathway regulates glucose metabolism. *Immunity* **16**, 769–777 (2002).
6. R. D. Cahn, E. Zwilling, N. O. Kaplan, L. Levine, Nature and development of lactic dehydrogenases: The two major types of this enzyme form molecular hybrids which change in makeup during development. *Science* **136**, 962–969 (1962).
7. R. Wang, C. P. Dillon, L. Z. Shi, S. Milasta, R. Carter, D. Finkelstein, L. L. McCormick, P. Fitzgerald, H. Chi, J. Munger, D. R. Green, The transcription factor Myc controls metabolic reprogramming upon T lymphocyte activation. *Immunity* **35**, 871–882 (2011).
8. L. Z. Shi, R. Wang, G. Huang, P. Vogel, G. Neale, D. R. Green, H. Chi, HIF1alpha-dependent glycolytic pathway orchestrates a metabolic checkpoint for the differentiation of TH17 and Treg cells. *J. Exp. Med.* **208**, 1367–1376 (2011).
9. A. Carreau, B. El Hafny-Rahbi, A. Matejuk, C. Grillon, C. Kieda, Why is the partial oxygen pressure of human tissues a crucial parameter? Small molecules and hypoxia. *J. Cell Mol. Med.* **15**, 1239–1253 (2011).
10. R. G. Jones, C. B. Thompson, Revving the engine: Signal transduction fuels T cell activation. *Immunity* **27**, 173–178 (2007).
11. K. Xu, N. Yin, M. Peng, E. G. Stamatiades, S. Chhangawala, A. Shyu, P. Li, X. Zhang, M. H. Do, K. J. Capistrano, C. Chou, C. S. Leslie, M. O. Li, Glycolytic ATP fuels phosphoinositide 3-kinase signaling to support effector T helper 17 cell responses. *Immunity* **54**, 976–987.e7 (2021).
12. M. Peng, N. Yin, S. Chhangawala, K. Xu, C. S. Leslie, M. O. Li, Aerobic glycolysis promotes T helper 1 cell differentiation through an epigenetic mechanism. *Science* **354**, 481–484 (2016).
13. M. A. Leney-Greene, A. K. Boddapati, H. C. Su, J. R. Cantor, M. J. Lenardo, Human plasma-like medium improves T lymphocyte activation. *iScience* **23**, 100759 (2020).
14. I. Kaymak, K. M. Luda, L. R. Duimstra, E. H. Ma, J. Longo, M. S. Dahabieh, B. Faubert, B. M. Oswald, M. J. Watson, S. M. Kitchen-Goosen, L. M. DeCamp, S. E. Compton, Z. Fu, R. J. DeBerardinis, K. S. Williams, R. D. Sheldon, R. G. Jones, Carbon source availability drives nutrient utilization in CD8(+) T cells. *Cell Metab.* **34**, 1298–1311.e6 (2022).
15. J. R. Cantor, M. Abu-Remaileh, N. Kanarek, E. Freinkman, X. Gao, A. Louissaint Jr., C. A. Lewis, D. M. Sabatini, Physiologic medium rewires cellular metabolism and reveals uric acid as an endogenous inhibitor of UMP synthase. Cell 169, 258–272.e17 (2017).
16. R. D. Michalek, V. A. Gerriets, S. R. Jacobs, A. N. Macintyre, N. J. MacIver, E. F. Mason, S. A. Sullivan, A. G. Nichols, J. C. Rathmell, Cutting edge: Distinct glycolytic and lipid oxidative metabolic programs are essential for effector and regulatory CD4$^+$ T cell subsets. *J. Immunol.* **186**, 3299–3303 (2011).

Downloaded from https://www.science.org on April 09, 2025

17. V. A. Gerriets, R. J. Kishton, A. G. Nichols, A. N. Macintyre, M. Inoue, O. Ilkayeva, P. S. Winter, X. Liu, B. Priyadharshini, M. E. Slawinska, L. Haeberli, C. Huck, L. A. Turka, K. C. Wood, L. P. Hale, P. A. Smith, M. A. Schneider, N. J. MacIver, J. W. Locasale, C. B. Newgard, M. L. Shinohara, J. C. Rathmell, Metabolic programming and PDHK1 control $CD4^+$ T cell subsets and inflammation. *J. Clin. Invest.* **125**, 194–207 (2015).
18. R. Wang, D. R. Green, Metabolic reprogramming and metabolic dependency in T cells. *Immunol. Rev.* **249**, 14–26 (2012).
19. H. A. Krebs, R. L. Veech, Equilibrium relations between pyridine nucleotides and adenine nucleotides and their roles in the regulation of metabolic processes. *Adv. Enzyme Regul.* **7**, 397–413 (1969).
20. D. H. Williamson, P. Lund, H. A. Krebs, The redox state of free nicotinamide-adenine dinucleotide in the cytoplasm and mitochondria of rat liver. *Biochem. J.* **103**, 514–527 (1967).
21. L. A. O'Neill, R. J. Kishton, J. Rathmell, A guide to immunometabolism for immunologists. *Nat. Rev. Immunol.* **16**, 553–565 (2016).
22. N. M. Chapman, M. R. Boothby, H. Chi, Metabolic coordination of T cell quiescence and activation. *Nat. Rev. Immunol.* **20**, 55–70 (2020).
23. A. T. Waickman, J. D. Powell, mTOR, metabolism, and the regulation of T-cell differentiation and function. *Immunol. Rev.* **249**, 43–58 (2012).
24. E. L. Pearce, M. C. Poffenberger, C. H. Chang, R. G. Jones, Fueling immunity: Insights into metabolism and lymphocyte function. *Science* **342**, 1242454 (2013).
25. M. D. Buck, R. T. Sowell, S. M. Kaech, E. L. Pearce, Metabolic instruction of immunity. *Cell* **169**, 570–586 (2017).
26. Z. Khan, M. J. Ford, D. A. Cusanovich, A. Mitrano, J. K. Pritchard, Y. Gilad, Primate transcript and protein expression levels evolve under compensatory selection pressures. *Science* **342**, 1100–1104 (2013).
27. T. Wolf, W. Jin, G. Zoppi, I. A. Vogel, M. Akhmedov, C. K. E. Bleck, T. Beltraminelli, J. C. Rieckmann, N. J. Ramirez, M. Benevento, S. Notarbartolo, D. Bumann, F. Meissner, B. Grimbacher, M. Mann, A. Lanzavecchia, F. Sallusto, I. Kwee, R. Geiger, Dynamics in protein translation sustaining T cell preparedness. *Nat. Immunol.* **21**, 927–937 (2020).
28. A. J. M. Howden, J. L. Hukelmann, A. Brenes, L. Spinelli, L. V. Sinclair, A. I. Lamond, D. A. Cantrell, Quantitative analysis of T cell proteomes and environmental sensors during T cell differentiation. *Nat. Immunol.* **20**, 1542–1554 (2019).
29. P. M. Gubser, G. R. Bantug, L. Razik, M. Fischer, S. Dimeloe, G. Hoenger, B. Durovic, A. Jauch, C. Hess, Rapid effector function of memory $CD8^+$ T cells requires an immediate-early glycolytic switch. *Nat. Immunol.* **14**, 1064–1072 (2013).
30. A. T. Johnson, Teaching the principle of biological optimization. *J Biol. Eng.* **7**, 6 (2013).
31. N. D. Bhattacharyya, C. G. Feng, Regulation of T Helper Cell Fate by TCR Signal Strength. *Front. Immunol.* **11**, 624 (2020).
32. N. R. Gascoigne, V. Rybakin, O. Acuto, J. Brzostek, TCR signal strength and T cell development. *Annu. Rev. Cell Dev. Biol.* **32**, 327–348 (2016).
33. E. L. Pearce, M. C. Walsh, P. J. Cejas, G. M. Harms, H. Shen, L. S. Wang, R. G. Jones, Y. Choi, Enhancing CD8 T-cell memory by modulating fatty acid metabolism. *Nature* **460**, 103–107 (2009).
34. W. J. Quinn 3rd, J. Jiao, T. TeSlaa, J. Stadanlick, Z. Wang, L. Wang, T. Akimova, A. Angelin, P. M. Schafer, M. D. Cully, C. Perry, P. K. Kopinski, L. Guo, I. A. Blair, L. R. Ghanem, M. S. Leibowitz, W. W. Hancock, E. K. Moon, M. H. Levine, E. B. Eruslanov, D. C. Wallace, J. A. Baur, U. H. Beier, Lactate limits T cell proliferation via the NAD(H) redox state. *Cell Rep.* **33**, 108500 (2020).
35. M. G. Vander Heiden, R. J. DeBerardinis, Understanding the intersections between metabolism and cancer biology. *Cell* **168**, 657–669 (2017).
36. C. V. Dang, MYC, metabolism, cell growth, and tumorigenesis. *Cold Spring Harb. Perspect. Med.* **3**, a014217 (2013).
37. R. J. DeBerardinis, N. S. Chandel, Fundamentals of cancer metabolism. *Sci. Adv.* **2**, e1600200 (2016).
38. W. Xiao, R.-S. Wang, D. E. Handy, J. Loscalzo, NAD(H) and NADP(H) redox couples and cellular energy metabolism. *Antioxid. Redox Signal.* **28**, 251–272 (2018).
39. H. Kong, N. S. Chandel, Regulation of redox balance in cancer and T cells. *J. Biol. Chem.* **293**, 7499–7507 (2018).
40. J. D. Rabinowitz, S. Enerback, Lactate: The ugly duckling of energy metabolism. *Nat. Metab.* **2**, 566–571 (2020).
41. L. B. Gladden, Lactate metabolism: A new paradigm for the third millennium. *J. Physiol.* **558**, 5–30 (2004).
42. X. Chen, J. W. Sherman, R. Wang, Radioisotope-based protocol for determination of central carbon metabolism in T cells. *Methods Mol. Biol.* **2111**, 257–265 (2020).

Acknowledgments: We thank M. Davis for assistance in editing the manuscript. **Funding:** This work was supported by 1UO1CA232488-01 from the NIH (Cancer Moonshot program), 2R01AI114581-06 and RO1CA247941 from the NIH, V2014-001 from the V-Foundation, 128436-RSG-15-180-01-LIB from the American Cancer Society (to R.W.), and T32 Ruth L. Kirschstein National Research Service Award CA269052 from the NIH (to S.K.). **Author contributions:** R.W. conceptualized and supervised this work. X.C., L.L., S.K., and J.N.R.G. carried out the experiments. X.C., L.L., S.K., and J.N.R.G. were involved in data collection, analysis, and review. R.W. and X.C. wrote the manuscript. All authors discussed the results and provided feedback on the manuscript. **Competing interests:** The authors declare that they have no competing interest. **Data and materials availability:** All data needed to evaluate the conclusions in the paper are present in the paper and/or the Supplementary Materials. The RNA sequencing datasets generated for this study can be found in the GEO accession GSE190799. The reagents can be provided by the corresponding author pending scientific review and a completed material transfer agreement.

Submitted 15 July 2022
Accepted 21 February 2023
Published 24 March 2023
10.1126/sciadv.add9554

Downloaded from https://www.science.org on April 09, 2025